Maximum *a Posteriori* Video Super-Resolution Using a New Multichannel Image Prior

Stefanos P. Belekos, *Member, IEEE*, Nikolaos P. Galatsanos, *Senior Member, IEEE*, and Aggelos K. Katsaggelos, *Fellow, IEEE*

***Abstract*—Super-resolution (SR) is the term used to define the process of estimating a high-resolution (HR) image or a set of HR images from a set of low-resolution (LR) observations. In this paper we propose a class of SR algorithms based on the maximum *a posteriori* (MAP) framework. These algorithms utilize a new multichannel image prior model, along with the state-of-the-art single channel image prior and observation models. A hierarchical (two-level) Gaussian nonstationary version of the multichannel prior is also defined and utilized within the same framework. Numerical experiments comparing the proposed algorithms among themselves and with other algorithms in the literature, demonstrate the advantages of the adopted multichannel approach.**

***Index Terms*—Image restoration, maximum *a posteriori* (MAP) framework, motion field estimation, multichannel prior, observation model, parameter estimation, super-resolution, video applications.**

I. Introduction

RESOLUTION enhancement of an image or a frame of a video sequence based on multiple LR observed frames, which is also referred to in the literature as *super-resolution (SR)*, is of critical importance in signal processing applications, such as video surveillance, remote sensing and medical imaging (e.g., X-rays). It has also been implemented in various consumer electronic products, such as, cell phones, digital video cameras, portable digital versatile disks (DVD), portable global positioning systems (GPSs), and high definition televisions (HDTVs) [1]–[5]. In each of these systems, the image resolution can be increased by using a higher-resolution sensor. However, in addition to cost considerations, the noise increases as the charge-coupled device (CCD) cell size decreases. Therefore, one must turn to algorithmic techniques to achieve resolution as well as quality enhancement [6].

A recent review of the SR field can be found in [4] and the references therein. The idea of SR was first formulated in the frequency domain [7], and it was extended in [8] and [9]. Some of the most recently proposed frequency domain methods are those in [10]–[12]. Although such methods are theoretically simple and computationally efficient, their use is limited by the fact that they are sensitive to modeling nonglobal translational motion, and they are not able to incorporate any spatial domain *prior knowledge* in their formulation [13].

In addition to these methods, another popular class of SR methods has been developed in the spatial domain, in order to overcome the aforementioned drawbacks. Typical examples of such approaches are based on iterative planar motion estimation algorithms [14], back-projection algorithms (IBP) [15], projection onto convex sets (POCS) [16], [17], maximum-likelihood (ML) [18] and maximum *a posteriori* (MAP) [19], [20]. However, the spatial domain methods are in general computationally expensive. Finally, wavelet based SR methods have also been proposed which are very robust to noise [21].

The SR problem is an ill-posed inverse problem that requires regularization. The Bayesian framework, used in this work, offers many advantages (see [4], for example). In most of the Bayesian formulations which have been used for developing SR algorithms so far, single channel (frame) image priors have been adopted, based on a Gaussian stationary assumption for the local image differences [22], [23] whereas there have also been proposed both non Bayesian [24]–[26] and Bayesian [27] total variation (TV) regularization techniques. As far as the imaging models are concerned, many techniques are incorporating the motion field (MF) information [22], [24], [25], [28], whereas others do not use this information at all.

The term multichannel [29] in the context of video recovery implies the use of the between frames correlation. Multichannel approaches have been used successfully in the past for video restoration [28]–[30] and compressed video reconstruction applications [31]. However, most of these approaches were deterministic and the multichannel idea was basically imposed by using between frame regularization.

In this paper, we address the video SR problem utilizing a MAP approach. One of the main contributions of this work is

Manuscript received October 07, 2008; revised January 03, 2010. First published February 02, 2010; current version published May 14, 2010. The associate editor coordinating the review of this manuscript and approving it for publication was Dr. Luminita Vese. This work was supported in part by the 03ED-535 research project, implemented within the framework of the Reinforcement Programme of Human Research Manpower (PENED) and co-financed by National and Community Funds (25% from the Greek Ministry of Development-General Secretariat of Research and Technology and 75% from E.U.-European Social Fund). S. P. Belekos performed part of this work while at Northwestern University, Image and Video Processing Laboratory, Department of Electrical Engineering and Computer Science, Evanston, IL 60208-3118 USA. This work was presented in part at the EUSIPCO, Lausanne, Switzerland, 2008. The associate editor coordinating the review of this manuscript and approving it for publication was Dr. Luminita Vese.

S. P. Belekos is with the Faculty of Physics, Department of Electronics, Computers, Telecommunications and Control, National and Kapodistrian University of Athens, Panepistimiopolis, Zografos, 15784 Athens, Greece (e-mail: stefbel@phys.uoa.gr).

N. P. Galatsanos is with the Department of Electrical and Computer Engineering, University of Patras, 26500 Rio, Greece (e-mail: ngalatsanos@upatras.gr).

A. K. Katsaggelos is with the Department of Electrical Engineering and Computer Science, Northwestern University, Evanston, IL 60208 USA, and also with the Faculty of Physics, National and Kapodistrian University of Athens, Greece (e-mail: aggk@eecs.northwestern.edu).

Digital Object Identifier 10.1109/TIP.2010.2042115

the introduction of a new multichannel prior that incorporates registration information between frames. Accurate registration of each pixel (dense MF) of adjacent frames is critical for the video SR reconstruction. An additional novelty factor of our work, consists in using the nonstationary image prior which was introduced in [32], in the SR problem. Consequently, a new single frame MAP SR algorithm is derived. Furthermore, this prior was also incorporated in the video resolution enhancement algorithm which was proposed in [22] and [23], resulting in a new proposed MAP SR technique for uncompressed video.

Moreover, we also introduce a nonstationary version of the aforementioned new multichannel prior within the MAP framework. In particular, we propose a novel SR algorithm that utilizes a hierarchical (two-level) Gaussian type prior which assumes that the residuals of first order differences (FODs) *within* each frame in *two directions* are Gaussian random variables (RVs) with zero mean and variance that is *spatially varying* [32]. The *same modeling assumption is made for each motion compensation error between every two frames which are used in the proposed prior*. In order to deal with the resulting overparameterization, the spatially varying variances (at each pixel location) are considered RVs and a Gamma hyperprior is imposed on each of them (whose mean and variance is controlled by the shape and scale parameters). Comparison among all these three proposed algorithms also indicates the relative advantage of the MF utilization in the prior term with respect to its use in the observation term.

The paper is organized as follows. In the next section, we present the appropriate mathematical background on all observation models and image priors used. In Section III, we introduce a general MAP problem formulation for the SR of uncompressed video regarding the proposed models, along with the corresponding algorithms. In Section IV, we provide numerical experiments that test the proposed methods. Finally, Section V presents the conclusions along with future work recommendations.

II. Mathematical Background

A. Observation Models

In this paper, we use two different observation models. In the first one the relationship between the $MN \times 1$ LR observation frame $\mathbf{g}_i$ and its $LMLN \times 1$ (L denotes the resolution enhancement factor) HR counterpart $\mathbf{f}_i$ is given in matrix-vector form by (all images have been lexicographically ordered)

$$\mathbf{g}_i = \mathbf{DHf}_i + \mathbf{n}_i, \quad \text{for } i = 1, 2 \ldots P \tag{1}$$

where $\mathbf{D}$ is the $MN \times LMLN$ down-sampling matrix, $\mathbf{H}$ is the $LMLN \times LMLN$ known blurring matrix, $\mathbf{n}_i$ of size $MN \times 1$, represents the additive white Gaussian noise (AWGN) term, and P represents the total number of frames used.

Equation (1) can be rewritten as

$$\tilde{\mathbf{g}} = \tilde{\mathbf{D}}\tilde{\mathbf{H}}\tilde{\mathbf{f}} + \tilde{\mathbf{n}} \tag{2}$$

where

$$\begin{aligned} \tilde{\mathbf{g}} &= \left[\mathbf{g}_{k-m}^T, \ldots, \mathbf{g}_k^T, \ldots, \mathbf{g}_{k+n}^T\right]^T \\ \tilde{\mathbf{f}} &= \left[\mathbf{f}_{k-m}^T, \ldots, \mathbf{f}_k^T, \ldots, \mathbf{f}_{k+n}^T\right]^T \\ \tilde{\mathbf{n}} &= \left[\mathbf{n}_{k-m}^T, \ldots, \mathbf{n}_k^T, \ldots, \mathbf{n}_{k+n}^T\right]^T \end{aligned} \tag{3}$$

n, m indicate, respectively, the number of frames used in the forward and backward temporal directions with respect to the kth frame ($n + m + 1 = P$), T denotes the transpose of a matrix or vector, and

$$\tilde{\mathbf{H}} = \text{diag}\{\mathbf{H}, \ldots, \mathbf{H}, \ldots, \mathbf{H}\}, \tilde{\mathbf{D}} = \text{diag}\{\mathbf{D}, \ldots, \mathbf{D}, \ldots, \mathbf{D}\} \tag{4}$$

are respectively of dimensions $PLMLN \times PLMLN$ and $PMN \times PLMLN$.

The second imaging model (warp-blur model [4]) used in this paper, is defined as

$$\mathbf{g}_i = \mathbf{DHM}(\mathbf{d}_{i,k})\mathbf{f}_k + \mathbf{w}_{i,k}, \quad \text{for } i = k-m, \ldots, k, \ldots, k+m \tag{5}$$

with $\mathbf{w}_{i,k} = \mathbf{n}_i + \mathbf{DHn}_{i,k}$ a column vector of size $MN \times 1$ representing *the total contribution* of the noise term (including both registration and acquisition errors) which is again modelled as AWGN (without lack of generality we have assumed that $m = n$). Moreover, $\mathbf{M}(\mathbf{d}_{i,k})$ is the 2-D motion compensation matrix of size $LMLN \times LMLN$, mapping frame $\mathbf{f}_k$ into frame $\mathbf{f}_i$ with the use of $\mathbf{d}_{i,k}$ (displacements at each pixel location). Here, using the imaging model in (5) we are using only the motion information that is relevant for the resolution enhancement of the kth frame. The assumption of AWGN is also adopted in [33] and [34], where a similar observation model is used. At this point, it is also mentioned that the non-AWGN assumption employed in [18] for the respective noise term is valid only for the special case of global motion [33]. This is not a restriction we are imposing in this work.

B. Image Prior Models

Although deterministic approaches have been developed in the past for video SR applications [24], [25], [35], the Bayesian formulation, which utilizes an image prior, offers many advantages. A simultaneously autoregressive (SAR) model has been used as an image prior for video SR [22]. This model is based on the assumption that the local image differences follow the same statistics all over the image. This assumption induces a prior for the image which has been used extensively in image recovery problems. It is very effective because it contains only one parameter (the within channel inverse variance/precision) resulting in easy analytical calculations. However, because of this (one parameter) it cannot capture the local properties of the image. One way to bypass this difficulty, as we shall see in what follows, is to introduce a prior with a spatially varying precision paremeter [32], [36]. In order to avoid the over parameterization problem, all of them are assumed to originate from the same conjugate Gamma probability density function (pdf).

In this work, we extend these ideas to the video SR problem. We, thus, propose a *new spatially adaptive (nonstationary) multichannel prior*. This model takes into account both the

within frame smoothness (spatial residuals) and the between-frame smoothness (temporal residuals). In this case, the respective regularization parameters are assumed to be *spatially varying* RVs and a Gamma hyperprior is imposed on *each* of them.

More specifically, based on [32], we introduce a hierarchical (two-level) Gaussian prior to model both its within channel and between-channel smoothness. The first step is to define the within channel FODs as $\boldsymbol{\varepsilon}_j^d = \mathbf{Q}^d\mathbf{f}_j$, where $d = 1, 2$ denotes the directions of 0° and 90°, respectively, and $\mathbf{Q}^d$ is the $LMLN \times LMLN$ *directional* difference operators for each frame. We now assume that the FODs at each spatial location and direction have Gaussian statistics (a commonly used assumption even in the case of spatially invariant FODs, see [37], for example) according to $\varepsilon_{j,\mu}^d \sim N(0, (\alpha_{j,\mu}^d)^{-1})$, where μ defines the pixel location and $\alpha_{j,\mu}^d$ is the inverse variance. For compactness of the presentation, we set $\boldsymbol{\alpha}_j^d = [\alpha_{j,1}^d, \alpha_{j,2}^d, \ldots, \alpha_{j,LMLN}^d]^T$, $\boldsymbol{\alpha}_j = [(\boldsymbol{\alpha}_j^{d=1})^T, (\boldsymbol{\alpha}_j^{d=2})^T]^T$ and $\boldsymbol{\alpha}^{\text{total}} = [\boldsymbol{\alpha}_{k-m}^T, \ldots, \boldsymbol{\alpha}_k^T, \ldots, \boldsymbol{\alpha}_{k+m}^T]^T$. Moreover, we introduce the notation $\mathbf{A}_j^d = \text{diag}\{\alpha_{j,1}^d, \alpha_{j,2}^d, \ldots, \alpha_{j,LMLN}^d\}$, where each matrix $\mathbf{A}_j^d$ for $d = 1, 2$ is of dimensions $LMLN \times LMLN$.

Assuming that the errors *at each direction and at each pixel location are independent* we obtain the following improper pdf [32]:

$$p(\mathbf{f}_j|\boldsymbol{\alpha}_j) \propto \prod_{d=1}^{2}\left(\prod_{\mu=1}^{LMLN}\left(\alpha_{j,\mu}^d\right)^{1/4}\right) \times \exp\left(-\frac{1}{2}\left((\mathbf{Q}^d\mathbf{f}_j)^T\mathbf{A}_j^d\mathbf{Q}^d\mathbf{f}_j\right)\right). \quad (6)$$

The independency assumption is based on the fact that at each pixel location an edge can occur in any direction independently of what happens in adjacent pixels and it also makes subsequent calculations tractable. Furthermore, improper priors are used on a routinely basis with success in Bayesian modeling (see [38], for example).

Moreover, a Gamma hyperprior is placed on each inverse variance (precision) $\alpha_{j,\mu}^d$, according to

$$p\left(\alpha_{j,\mu}^d; \nu_j^d, l_j^d\right) \propto \left(\alpha_{j,\mu}^d\right)^{\frac{l_j^d-2}{2}} \exp\left(-\nu_j^d\left(l_j^d-2\right)\alpha_{j,\mu}^d\right) \quad (7)$$

where $E[\alpha_{j,\mu}^d] = l_j^d(2\nu_j^d(l_j^d-2))^{-1}$, $\text{Var}[\alpha_{j,\mu}^d] = l_j^d(2(\nu_j^d)^2(l_j^d-2)^2)^{-1}$, and ν_j^d, l_j^d are the scale and shape parameters, respectively, per frame and per direction [37], [39]. The rationale for using a Gamma prior on each inverse variance is threefold. First, it is "conjugate" for the variance of a Gaussian [40]. Second, similar hierarchical models have been used successfully in Bayesian formulations of other statistical learning problems [41]. Finally, as we shall see in the following, it produces compact equations for the inverse variances. Assuming also that the variances of the Gaussians modeling the residual errors are statistically independent, we have from (7)

$$p(\boldsymbol{\alpha}_j; \boldsymbol{\nu}_j, \boldsymbol{l}_j) = \prod_{d=1}^{2}\prod_{\mu=1}^{LMLN} p\left(\alpha_{j,\mu}^d; \nu_j^d, l_j^d\right) \quad (8)$$

where $\boldsymbol{\nu}_j = [\nu_j^{d=1}, \nu_j^{d=2}]^T$ and $\boldsymbol{l}_j = [l_j^{d=1}, l_j^{d=2}]^T$. This assumption allows these variances to scale down the differences of adjacent pixels not only in smooth areas, but also in regions of image discontinuities (e.g., edges). Therefore, combining (6) and (8), we obtain

$$p(\mathbf{f}_j, \boldsymbol{\alpha}_j; \boldsymbol{\nu}_j, \boldsymbol{l}_j) = p(\mathbf{f}_j|\boldsymbol{\alpha}_j)p(\boldsymbol{\alpha}_j; \boldsymbol{\nu}_j, \boldsymbol{l}_j) \quad (9)$$

representing the proposed within channel nonstationary prior.

We now define the proposed between-channel nonstationary prior. More specifically, we define each motion compensated error (residual) between two frames ($\boldsymbol{\delta}_{ij} = (\mathbf{f}_i - \mathbf{M}(\mathbf{d}_{i,j})\mathbf{f}_j)$, for $j \neq i$) *per pixel* as $\delta_{ij,\mu} \sim N(0, (\beta_{ij,\mu})^{-1})$. We also set $\boldsymbol{\beta}_{ij} = [\beta_{ij,1}, \beta_{ij,2}, \ldots, \beta_{ij,LMLN}]^T$, which is a column vector of size $LMLN \times 1$ and also $\boldsymbol{\beta}^{\text{total}} = [\boldsymbol{\beta}_{ij}^T]_{j\neq i}^T$ which is also a column vector of size $2m(2m+1)LMLN \times 1$ containing all possible precisions of the motion compensation errors and $2m(2m+1)$ equals the number of all possible channel combinations. Furthermore, we denote by $\mathbf{B}_{ij} = \text{diag}\{\beta_{ij,1}, \beta_{ij,2}, \ldots, \beta_{ij,LMLN}\}$, for $j \neq i$, where each such matrix is of size $LMLN \times LMLN$.

Following the framework in [32] and assuming that the motion compensation errors are *independent at each spatial location*, given that each pixel of one frame is predicted by a pixel of another frame independently of (the predictions of) its adjacent pixels, we obtain the following Gaussian motion compensation error pdf:

$$p(\mathbf{f}_i|\mathbf{f}_j, \boldsymbol{\beta}_{ij}) \propto \left(\prod_{\mu=1}^{LMLN}(\beta_{ij,\mu})^{1/2}\right) \times \exp\left(-\frac{1}{2}\left((\mathbf{f}_i - \mathbf{M}_{ij}\mathbf{f}_j)^T\mathbf{B}_{ij}(\mathbf{f}_i - \mathbf{M}_{ij}\mathbf{f}_j)\right)\right) \quad (10)$$

with the assumption

$$\mathbf{M}_{ji} = (\mathbf{M}_{ij})^T = \mathbf{M}(\mathbf{d}_{j,i}) \quad (11)$$

where matrix $(\mathbf{M}_{ij})^T$ represents the backward motion compensation operation along the motion vectors (mapping frame $\mathbf{f}_i$ into frame $\mathbf{f}_j$ with the use of $\mathbf{d}_{j,i}$). Note that (11) holds when the assumption of integer pixel accuracy MF holds, along with the one-to-one mapping through motion. In this case the motion compensation matrices are *indicator matrices of full rank* thus it also holds that $(\mathbf{M}_{ij})^T\mathbf{M}_{ij} = \mathbf{I}$ [30], or $\mathbf{M}_{ji}\mathbf{M}_{ij} = \mathbf{I}$.

A Gamma hyperprior is imposed on each such spatially varying precision, expressed as

$$p(\beta_{ij,\mu}; \tau_{ij}, \xi_{ij}) \propto (\beta_{ij,\mu})^{\frac{\xi_{ij}-2}{2}} \exp\left(-\tau_{ij}(\xi_{ij}-2)\beta_{ij,\mu}\right) \quad (12)$$

where $E[\beta_{ij,\mu}] = \xi_{ij}(2\tau_{ij}(\xi_{ij}-2))^{-1}$ and $\text{Var}[\beta_{ij,\mu}] = \xi_{ij}(2(\tau_{ij})^2(\xi_{ij}-2)^2)^{-1}$, and τ_{ij}, ξ_{ij} are the parameters per motion compensation error ($j \neq i$). Based on the assumption that the variances of the Gaussians modeling the errors are statistically independent and on (12), we obtain

$$p(\boldsymbol{\beta}_{ij}; \tau_{ij}, \xi_{ij}) = \prod_{\mu=1}^{LMLN} p(\beta_{ij,\mu}; \tau_{ij}, \xi_{ij}). \quad (13)$$

This assumption also stems from the fact that these variances scale down the compensation errors of adjacent pixels which can be located either in smooth areas or in edges, textures, etc.

In this new prior the value of each parameter l_j^d and ξ_{ij} is interpreted as the level of confidence on the information provided by each Gamma hyperprior. This is attributed to the fact that as $l_j^d \to \infty$, $E[\alpha_{j,\mu}^d] \to (2\nu_j^d)^{-1}$, $\mathrm{Var}[\alpha_{j,\mu}^d] \to 0$, and as $\xi_{ij} \to \infty$, $E[\beta_{ij,\mu}] \to (2\tau_{ij})^{-1}$, $\mathrm{Var}[\beta_{ij,\mu}] \to 0$, which means that *the prior becomes stationary*. In contrast, as both parameters l_j^d and $\xi_{ij} \to 2$ then all $E[\alpha_{j,\mu}^d]$, $E[\beta_{ij,\mu}]$, $\mathrm{Var}[\alpha_{j,\mu}^d]$ and $\mathrm{Var}[\beta_{ij,\mu}]$ go to infinity, thus the prior becomes *totally nonstationary* (uninformative) in both its within and cross-channel parts and does not influence at all the values of $\alpha_{j,\mu}^d$ and $\beta_{ij,\mu}$, which as a result follow only the data and the motion compensation trajectories, respectively. Consequently, the values of the parameters l_j^d and ξ_{ij} can be viewed as the only way to regulate the *degrees of freedom (nonstationarity)* of the proposed prior.

Combining (9), (10), and (13), the proposed spatially adaptive multichannel prior can be expressed as

$$\begin{aligned} p(\tilde{\mathbf{f}}, \boldsymbol{\alpha}^{\mathrm{total}}, \boldsymbol{\beta}^{\mathrm{total}}; \boldsymbol{\nu}^{\mathrm{total}}, \boldsymbol{l}^{\mathrm{total}}, \boldsymbol{\tau}^{\mathrm{total}}, \boldsymbol{\xi}^{\mathrm{total}}) & \\ \propto \prod_{i=k-m}^{k+m} \prod_{\substack{j=k-m \\ j\neq i}}^{k+m} p(\mathbf{f}_i, \mathbf{f}_j, \boldsymbol{\alpha}_j, \boldsymbol{\beta}_{ij}; \boldsymbol{\nu}_j, \boldsymbol{l}_j, \tau_{ij}, \xi_{ij}) & \\ = \prod_{i=k-m}^{k+m} \prod_{\substack{j=k-m \\ j\neq i}}^{k+m} p(\mathbf{f}_i|\mathbf{f}_j, \boldsymbol{\beta}_{ij}) p(\mathbf{f}_j|\boldsymbol{\alpha}_j) p(\boldsymbol{\alpha}_j; \boldsymbol{\nu}_j, \boldsymbol{l}_j) & \\ \times p(\boldsymbol{\beta}_{ij}; \tau_{ij}, \xi_{ij}) & \end{aligned} \tag{14}$$

where $\boldsymbol{\nu}^{\mathrm{total}}, \boldsymbol{l}^{\mathrm{total}}$ are defined similarly to $\boldsymbol{\alpha}^{\mathrm{total}}$, and $\boldsymbol{\tau}^{\mathrm{total}} = [\tau_{ij}]_{j\neq i}^T$, and $\boldsymbol{\xi}^{\mathrm{total}} = [\xi_{ij}]_{j\neq i}^T$ are column vectors of size $2m(2m+1) \times 1$ containing the hyperparameters for each motion compensation error.

If we write out (14), the term containing $\tilde{\mathbf{f}}$ is given by

$$\Phi(\tilde{\mathbf{f}}) = \exp\left[-\frac{1}{2}\sum_{i=k-m}^{k+m}\sum_{\substack{j=k-m \\ j\neq i}}^{k+m}\left[\left((\mathbf{f}_i - \mathbf{M}_{ij}\mathbf{f}_j)^T \mathbf{B}_{ij}(\mathbf{f}_i - \mathbf{M}_{ij}\mathbf{f}_j)\right) + \sum_{d=1}^{2}\left((\mathbf{Q}^d\mathbf{f}_j)^T \mathbf{A}_j^d (\mathbf{Q}^d\mathbf{f}_j)\right)\right]\right]. \tag{15}$$

In order to facilitate subsequent derivations, $\Phi(\tilde{\mathbf{f}})$ can be rewritten in a more compact form as

$$\begin{aligned} \Phi(\tilde{\mathbf{f}}) &= \exp\left[-\frac{1}{2}\sum_{i=k-m}^{k+m}\sum_{\substack{j=k-m \\ j\neq i}}^{k+m}\left[\mathbf{f}_i^T, \mathbf{f}_j^T\right]\boldsymbol{\Omega}_{ij}\begin{bmatrix}\mathbf{f}_i \\ \mathbf{f}_i\end{bmatrix}\right] \\ &= \exp\left[-\frac{1}{2}\tilde{\mathbf{f}}^T\tilde{\boldsymbol{\Omega}}\tilde{\mathbf{f}}\right] \end{aligned} \tag{16}$$

where

$$\begin{aligned} \boldsymbol{\Omega}_{ij} &= \begin{bmatrix} \mathbf{B}_{ij} & -\mathbf{B}_{ij}\mathbf{M}_{ij} \\ -(\mathbf{M}_{ij})^T\mathbf{B}_{ij} & \left[\sum_{d=1}^{2}\left[(\mathbf{Q}^d)^T\mathbf{A}_j^d\mathbf{Q}^d\right] + (\mathbf{M}_{ij})^T\mathbf{B}_{ij}\mathbf{M}_{ij}\right] \end{bmatrix} \\ &= \begin{bmatrix} \omega_{1,ij} & \omega_{ij} \\ \omega_{ij}'' & \omega_{2,ij} \end{bmatrix}. \end{aligned} \tag{17}$$

The construction of $\tilde{\boldsymbol{\Omega}}$ from $\boldsymbol{\Omega}_{ij}$ is a simple algebraic task based on (15), (16), and (17). For $k = 2$ and $m = 1$, it is easy to verify that $\tilde{\boldsymbol{\Omega}}$ is given by the expression in (18), shown at the bottom of the page. The presence of the compact term $\exp[-(1/2)\tilde{\mathbf{f}}^T\tilde{\boldsymbol{\Omega}}\tilde{\mathbf{f}}]$ makes calculations tractable as far as the estimation of $\tilde{\mathbf{f}}$ is concerned using the MAP algorithm, as discussed in the next section. Finally, $\tilde{\boldsymbol{\Omega}}$ is a symmetric matrix of size $PLMLN \times PLMLN$ which can be easily computed for any k and m.

The stationary version of the proposed prior is discussed next. As already mentioned, such a prior can be obtained in the *asymptotic* case when $l_j^d \to \infty$ and $\xi_{ij} \to \infty$. In this case, the new proposed spatially adaptive prior becomes *stationary* in the sense that both spatial (within channel) and temporal (between-channel) smoothness is uniformly enforced across the entire frame and across the motion compensation trajectories. The stationary version of (6) is expressed by

$$p(\mathbf{f}_j; \alpha_j) \propto \exp\left(-\frac{\alpha_j}{2}\|\mathbf{Q}\mathbf{f}_j\|^2\right) \tag{19}$$

where $\mathbf{Q}$ represents a linear high-pass convolutional operator (e.g., discrete Laplacian) of size $LMLN \times LMLN$, $\|\cdot\|$ denotes the l_2 norm and the parameter α_j accounts for the within channel inverse variance. Moreover, the stationary formulation of (10) can be obtained as

$$p(\mathbf{f}_i|\mathbf{f}_j; \beta_{ij}) \propto \exp\left(-\frac{\beta_{ij}}{2}\|\mathbf{f}_i - \mathbf{M}_{ij}\mathbf{f}_j\|^2\right). \tag{20}$$

Thus the stationary version of the proposed new multichannel prior is expressed as

$$p(\tilde{\mathbf{f}}; \tilde{\boldsymbol{\beta}}, \tilde{\boldsymbol{\alpha}}) \propto \prod_{i=k-m}^{k+m}\prod_{\substack{j=k-m \\ j\neq i}}^{k+m} p(\mathbf{f}_i|\mathbf{f}_j; \beta_{ij}) p(\mathbf{f}_j; \alpha_j) \tag{21}$$

where $p(\mathbf{f}_j; \alpha_j)$ is given by (19), with $\tilde{\boldsymbol{\beta}}$ and $\tilde{\boldsymbol{\alpha}}$ being column vectors that contain the parameters β_{ij} and α_j, respectively. Equation (21) can also be rewritten in a more compact form following the same algebraic steps as we did in the case of (14). In this case also, parameter β_{ij} represents the inverse variance (precision) of the motion compensation error between frames i and j.

$$\tilde{\boldsymbol{\Omega}} = \begin{bmatrix} \omega_{1,12} + \omega_{1,13} + \omega_{2,21} + \omega_{2,31} & \omega_{12} + \omega_{21}'' & \omega_{13} + \omega_{31}'' \\ \omega_{21} + \omega_{12}'' & \omega_{1,21} + \omega_{1,23} + \omega_{2,12} + \omega_{2,32} & \omega_{23} + \omega_{32}'' \\ \omega_{31} + \omega_{13}'' & \omega_{32} + \omega_{23}'' & \omega_{1,31} + \omega_{1,32} + \omega_{2,13} + \omega_{2,23} \end{bmatrix} \tag{18}$$

Finally, it is mentioned that in both versions of the new proposed priors expressed by (14) and (21), not all relations among frames in the $(2m+1)$ window are utilized. More specifically, each frame is conditioned on only one of the rest of the frames at a time and not on all of them. The use of more than one frames upon which to condition the current frame, on one hand it clearly introduces additional computations, while on the other hand it has been shown experimentally not to provide any additional performance benefits.

III. Proposed Algorithms

In this paper the MAP point estimate is utilized for recovering HR information from a sequence of low resolution observations. The MAP formulation for the SR problem of uncompressed video, is specified for each one of the proposed algorithms. It is given by

$$\begin{aligned}\hat{\tilde{\mathbf{f}}}, \hat{\boldsymbol{\alpha}}^{\text{total}}, \hat{\boldsymbol{\beta}}^{\text{total}} &= \underset{\tilde{\mathbf{f}}, \boldsymbol{\alpha}^{\text{total}}, \boldsymbol{\beta}^{\text{total}}}{\arg\max}\; p(\tilde{\mathbf{f}}, \boldsymbol{\alpha}^{\text{total}}, \boldsymbol{\beta}^{\text{total}} | \tilde{\mathbf{g}}; \tilde{\boldsymbol{\theta}}) \\ &= \underset{\tilde{\mathbf{f}}, \boldsymbol{\alpha}^{\text{total}}, \boldsymbol{\beta}^{\text{total}}}{\arg\max}\; \frac{p(\tilde{\mathbf{g}}, \tilde{\mathbf{f}}, \boldsymbol{\alpha}^{\text{total}}, \boldsymbol{\beta}^{\text{total}}; \tilde{\boldsymbol{\theta}})}{p(\tilde{\mathbf{g}})} \\ &= \underset{\tilde{\mathbf{f}}, \boldsymbol{\alpha}^{\text{total}}, \boldsymbol{\beta}^{\text{total}}}{\arg\max}\; \frac{p(\tilde{\mathbf{g}} | \tilde{\mathbf{f}}, \boldsymbol{\alpha}^{\text{total}}, \boldsymbol{\beta}^{\text{total}}; \tilde{\boldsymbol{\theta}}) p(\tilde{\mathbf{f}}, \boldsymbol{\alpha}^{\text{total}}, \boldsymbol{\beta}^{\text{total}}; \tilde{\boldsymbol{\theta}})}{p(\tilde{\mathbf{g}})}\end{aligned} \tag{22}$$

where $\tilde{\boldsymbol{\theta}}$ denotes the column vector that contains all the parameters $\boldsymbol{\nu}^{\text{total}}, \boldsymbol{l}^{\text{total}}, \boldsymbol{\tau}^{\text{total}}, \boldsymbol{\xi}^{\text{total}}$ along with the noise inverse variance parameters, whereas the RVs $\boldsymbol{\alpha}^{\text{total}}, \boldsymbol{\beta}^{\text{total}}$ are jointly estimated with the HR frames $\tilde{\mathbf{f}}$. Instead of the maximization in (22) the negative of the logarithm of $p(\tilde{\mathbf{f}}, \boldsymbol{\alpha}^{\text{total}}, \boldsymbol{\beta}^{\text{total}} | \tilde{\mathbf{g}}; \tilde{\boldsymbol{\theta}})$ with respect to $\tilde{\mathbf{f}}$, $\boldsymbol{\alpha}^{\text{total}}$, $\boldsymbol{\beta}^{\text{total}}$ and to the noise parameters is typically minimized.

By utilizing the observation models (1) and (5) and the prior models (9) and (14) (along with their respective stationary versions), we propose three formulations of the HR problem and derive the corresponding MAP algorithms. For each algorithm, we first provide its nonstationary formulation followed by the limiting stationary one.

A. Algorithm 1

The simplest observation model we can use is the one in (1), in which case no MF information is used. More specifically, each frame in the sequence is recovered independently from the other frames. The fidelity pdf then is defined as

$$p(\mathbf{g}_i | \mathbf{f}_i; \gamma_i) \propto \gamma_i^{\frac{MN}{2}} \exp\left(-\frac{\gamma_i}{2} \|\mathbf{g}_i - \mathbf{D}\mathbf{H}\mathbf{f}_i\|^2\right) \tag{23}$$

where the parameter γ_i^{-1} is the acquisition noise variance and the prior model is defined by (9).

The objective functional to be minimized for obtaining a MAP estimate is given by

$$\begin{aligned}J_{\text{MAP}}(\mathbf{f}_i, \boldsymbol{\alpha}_i | \mathbf{g}_i; \gamma_i, \boldsymbol{\nu}_i, \boldsymbol{l}_i) &\propto -2 \log p(\mathbf{g}_i, \mathbf{f}_i, \boldsymbol{\alpha}_i; \gamma_i, \boldsymbol{\nu}_i, \boldsymbol{l}_i) \\ &= -2 \log p(\mathbf{g}_i | \mathbf{f}_i, \boldsymbol{\alpha}_i; \gamma_i) \\ &\quad - 2 \log p(\mathbf{f}_i, \boldsymbol{\alpha}_i; \boldsymbol{\nu}_i, \boldsymbol{l}_i).\end{aligned} \tag{24}$$

Taking its partial derivatives with respect to $\mathbf{f}_i$, $\boldsymbol{\alpha}_i$ and γ_i and setting them equal to zero results in the following linear system of equations

$$\alpha_{i,\mu}^d = \frac{\left(\frac{1}{4} + \frac{1}{2}\left(l_i^d - 2\right)\right)}{\left(\frac{1}{2}\left(\varepsilon_{i,\mu}^d\right)^2 + \nu_i^d\left(l_i^d - 2\right)\right)} \tag{25}$$

$$\gamma_i = \frac{MN}{\|\mathbf{g}_i - \mathbf{D}\mathbf{H}\mathbf{f}_i\|^2} \tag{26}$$

$$\left(\mathbf{H}^T\mathbf{D}^T\mathbf{D}\mathbf{H} + \gamma_i^{-1}\sum_{d=1}^{2}\left(\mathbf{Q}^d\right)^T\mathbf{A}_i^d\mathbf{Q}^d\right)\hat{\mathbf{f}}_i = \mathbf{H}^T\mathbf{D}^T\mathbf{g}_i. \tag{27}$$

For the stationary algorithm, (25) and (27) reduce respectively to the following expressions:

$$\alpha_i = \frac{(LMLN - 1)}{\|\mathbf{Q}\mathbf{f}_i\|^2} \tag{28}$$

and

$$\left(\mathbf{H}^T\mathbf{D}^T\mathbf{D}\mathbf{H} + \frac{a_i}{\gamma_i}\mathbf{Q}^T\mathbf{Q}\right)\hat{\mathbf{f}}_i = \mathbf{H}^T\mathbf{D}^T\mathbf{g}_i \tag{29}$$

while (26) remains the same. These equations, are obtained based on the previous analysis and more specifically on the fact that as $l_i^d \to \infty$, $E[\alpha_{i,\mu}^d] \to (2\nu_i^d)^{-1}$ and $\text{Var}[\alpha_{j,\mu}^d] \to 0$ and consequently $E[\alpha_{i,\mu}^d]$ equals α_i (stationary prior model) and $\mathbf{A}_i^d = \alpha_i\mathbf{I}$.

The aforementioned algorithm is illustrated step by step as follows.

Algorithm 1: Single frame SR

Given an initial estimate for each HR image
while Convergence criterion is not met **do**
1) Estimate $\alpha_{i,\mu}^d$ using (25) -nonstationary prior- or α_i using (28) -stationary prior-
2) Estimate γ_i using (26)
3) Based on steps 1) and 2), estimate HR image using (27) -nonstationary prior- or (29) -stationary prior-

B. Algorithm 2

This algorithm is based on [22], where the observation model is now described by (5) and the prior model is also given by (9) as in Algorithm 1. That is, in this case the correlation between frames is captured by the observation model only, since the prior

model only considers one frame at a time. The fidelity pdf is given by

$$p(\mathbf{g}_i|\mathbf{f}_k;\gamma_{ik}) \propto \gamma_{ik}^{\frac{MN}{2}} \exp\left(-\frac{\gamma_{ik}}{2}||\mathbf{g}_i - \mathbf{DHM}_{ik}\mathbf{f}_k||^2\right) \quad (30)$$

where the parameters γ_{ik} are the inverse noise variances (precisions) related to both the motion compensation errors and the acquisition noise and as expected for $i = k$ it holds that $\gamma_{ik} = \gamma_i = \gamma_k$ in (23). Moreover, when $\mathbf{f}_k$ (and the MF matrices) are given, the RVs $\mathbf{g}_i$ (observations), or the respective error terms, are assumed to be *statistically* independent. Thus, we have

$$p(\tilde{\mathbf{g}}|\mathbf{f}_k;\tilde{\boldsymbol{\gamma}}) = \prod_{i=k-m}^{k+m} p(\mathbf{g}_i|\mathbf{f}_k, \mathbf{d}_{i,k}, \mathbf{d}_{k,i}; \gamma_{ik}) \quad (31)$$

where $\tilde{\boldsymbol{\gamma}}$ denotes the column vector that contains all (scalar) parameters γ_{ik}.

As far as the nonstationary form of this particular algorithm is concerned, the objective function that is minimized with respect to $\mathbf{f}_k$, $\boldsymbol{\alpha}_k$ and γ_{ik} is given by

$$\begin{aligned} &J_{\mathrm{MAP}}(\mathbf{f}_k, \boldsymbol{\alpha}_k|\tilde{\mathbf{g}};\tilde{\boldsymbol{\gamma}}) \\ &\quad \propto -2\log[p(\tilde{\mathbf{g}}|\mathbf{f}_k, \boldsymbol{\alpha}_k;\tilde{\boldsymbol{\gamma}})p(\mathbf{f}_k, \boldsymbol{\alpha}_k;\boldsymbol{\nu}_k, \boldsymbol{l}_k)] \\ &\quad = -2\log\left[\prod_{i=k-m}^{k+m} p(\mathbf{g}_i|\mathbf{f}_k, \boldsymbol{\alpha}_k, \mathbf{d}_{i,k}, \mathbf{d}_{k,i}; \gamma_{ik}) \right. \\ &\qquad\qquad \left. \times\, p(\mathbf{f}_k, \boldsymbol{\alpha}_k;\boldsymbol{\nu}_k, \boldsymbol{l}_k)\right] \\ &\quad = -2\log\left[\prod_{i=k-m}^{k+m} p(\mathbf{g}_i|\mathbf{f}_k, \boldsymbol{\alpha}_k, \mathbf{d}_{i,k}, \mathbf{d}_{k,i}; \gamma_{ik})\right] \\ &\qquad - 2\log[p(\mathbf{f}_k, \boldsymbol{\alpha}_k;\boldsymbol{\nu}_k, \boldsymbol{l}_k)] \end{aligned} \quad (32)$$

resulting in

$$\gamma_{ik} = \frac{MN}{||\mathbf{g}_i - \mathbf{DHM}_{ik}\mathbf{f}_k||^2} \quad (33)$$

$$\left(\tilde{\mathbf{J}} + \sum_{d=1}^{2} (\mathbf{Q}^d)^T \mathbf{A}_k^d \mathbf{Q}^d\right) \hat{\mathbf{f}}_k = \tilde{\mathbf{Z}} \quad (34)$$

with

$$\tilde{\mathbf{J}} = \sum_{i=k-m}^{k+m} \left[\gamma_{ik}(\mathbf{M}_{ki}\mathbf{H}^T\mathbf{D}^T\mathbf{DHM}_{ik})\right] \quad (35)$$

$$\tilde{\mathbf{Z}} = \sum_{i=k-m}^{k+m} \left[\gamma_{ik}(\mathbf{M}_{ki}\mathbf{H}^T\mathbf{D}^T\mathbf{g}_i)\right] \quad (36)$$

where $\alpha_{k,\mu}^d$ to be used in $\mathbf{A}_k^d$ is given by the right-hand side of (25). Clearly with this algorithm, only the MFs which are relevant to the HR frame $\hat{\mathbf{f}}_k$ are used. Moreover, as expected, the nonstationarity of Algorithms 1 and 2 is exclusively determined by the within channel nonstationary part of the respective proposed prior, which is expressed by (9). Based on the same arguments made in reference to Algorithm 1, the stationary version of Algorithm 2 (34) reduces to

$$(\tilde{\mathbf{J}} + a_k\mathbf{Q}^T\mathbf{Q})\hat{\mathbf{f}}_k = \tilde{\mathbf{Z}} \quad (37)$$

where the estimation of the parameter a_k is given by (28) and (33) remains unaffected.

The corresponding algorithm can be given in a compact form as follows.

Algorithm 2

Given an initial estimate for each HR image

1) Estimate the required MFs
2) Estimate $\alpha_{k,\mu}^d$ using (25) -nonstationary prior- or α_k using (28) -stationary prior-
3) Estimate γ_{ik} using (33)
4) Based on steps 1), 2) and 3) estimate HR image using (34) -nonstationary prior- or (37) -stationary prior-

C. Algorithm 3

Utilizing this algorithm the observation term described by (2) is combined with the new *multichannel prior* described by (14). That is, in this case the frame correlation as described by the MF, is captured by the prior model and not in the observation model.

In this case, the fidelity term is given by

$$\begin{aligned} p(\tilde{\mathbf{g}}|\tilde{\mathbf{f}};\tilde{\boldsymbol{\gamma}}) \propto &\left(\det\{\tilde{\boldsymbol{\Gamma}}\}\right)^{-\frac{1}{2}} \\ &\times \exp\left\{-\frac{1}{2}(\tilde{\mathbf{g}} - \tilde{\mathbf{D}}\tilde{\mathbf{H}}\tilde{\mathbf{f}})^T\tilde{\boldsymbol{\Gamma}}^{-1}(\tilde{\mathbf{g}} - \tilde{\mathbf{D}}\tilde{\mathbf{H}}\tilde{\mathbf{f}})\right\} \end{aligned} \quad (38)$$

where $\tilde{\boldsymbol{\Gamma}} = \mathrm{diag}\{\gamma_{k-m}^{-1}\mathbf{I}, \ldots, \gamma_k^{-1}\mathbf{I}, \ldots, \gamma_{k+m}^{-1}\mathbf{I}\}$ is the covariance matrix of size $PMN \times PMN$, $\mathbf{I}$ is the identity matrix of size $MN \times MN$ and $\tilde{\boldsymbol{\gamma}} = [\gamma_{k-m}, \ldots, \gamma_k, \ldots, \gamma_{k+m}]^T$ is the column vector that contains the inverse noise variances for each one of the channels that are used.

Consequently, the objective function is expressed as

$$\begin{aligned} &J_{\mathrm{MAP}}(\tilde{\mathbf{f}}, \boldsymbol{\alpha}^{\mathrm{total}}, \boldsymbol{\beta}^{\mathrm{total}}|\tilde{\mathbf{g}};\boldsymbol{\nu}^{\mathrm{total}}, \boldsymbol{l}^{\mathrm{total}}, \boldsymbol{\tau}^{\mathrm{total}}, \boldsymbol{\xi}^{\mathrm{total}}, \tilde{\boldsymbol{\gamma}}) \\ &\quad \propto -2\log p(\tilde{\mathbf{g}}, \tilde{\mathbf{f}}, \boldsymbol{\alpha}^{\mathrm{total}}, \boldsymbol{\beta}^{\mathrm{total}};\boldsymbol{\nu}^{\mathrm{total}}, \boldsymbol{l}^{\mathrm{total}}, \boldsymbol{\tau}^{\mathrm{total}}, \boldsymbol{\xi}^{\mathrm{total}}\tilde{\boldsymbol{\gamma}}) \\ &\quad = -2\log p(\tilde{\mathbf{g}}|\tilde{\mathbf{f}}, \boldsymbol{\alpha}^{\mathrm{total}}, \boldsymbol{\beta}^{\mathrm{total}};\tilde{\boldsymbol{\gamma}}) \\ &\qquad - 2\log p(\tilde{\mathbf{f}}, \boldsymbol{\alpha}^{\mathrm{total}}, \boldsymbol{\beta}^{\mathrm{total}};\boldsymbol{\nu}^{\mathrm{total}}, \boldsymbol{l}^{\mathrm{total}}, \boldsymbol{\tau}^{\mathrm{total}}, \boldsymbol{\xi}^{\mathrm{total}}). \end{aligned} \quad (39)$$

Its minimization with respect to $\beta_{ij,\mu}$, $\tilde{\mathbf{f}}$, $\alpha_{j,\mu}^d$ and γ_j yields

$$\beta_{ij,\mu} = \frac{\left(\frac{1}{2} + \frac{1}{2}(\xi_{ij} - 2)\right)}{\left(\frac{1}{2}(\delta_{ij,\mu})^2 + \tau_{ij}(\xi_{ij} - 2)\right)} \quad (40)$$

and

$$(\tilde{\mathbf{G}} + \tilde{\boldsymbol{\Omega}})\hat{\tilde{\mathbf{f}}} = \tilde{\Lambda}\tilde{\mathbf{g}} \quad (41)$$

where

$$\begin{aligned}\tilde{\mathbf{G}} &= \tilde{\mathbf{H}}^T\tilde{\mathbf{D}}^T\tilde{\mathbf{\Gamma}}^{-1}\tilde{\mathbf{D}}\tilde{\mathbf{H}} \\ &= \mathrm{diag}\{\gamma_{k-m}\mathbf{H}^T\mathbf{D}^T\mathbf{D}\mathbf{H},\ldots,\gamma_k\mathbf{H}^T\mathbf{D}^T\mathbf{D}\mathbf{H}, \\ &\qquad \ldots\gamma_{k+m}\mathbf{H}^T\mathbf{D}^T\mathbf{D}\mathbf{H}\}, \end{aligned} \tag{42}$$

$$\begin{aligned}\tilde{\Lambda} &= \tilde{\mathbf{H}}^T\tilde{\mathbf{D}}^T\tilde{\mathbf{\Gamma}}^{-1} \\ &= \mathrm{diag}\{\gamma_{k-m}\mathbf{H}^T\mathbf{D}^T,\ldots,\gamma_k\mathbf{H}^T\mathbf{D}^T, \\ &\qquad \ldots,\gamma_{k+m}\mathbf{H}^T\mathbf{D}^T\}, \end{aligned} \tag{43}$$

$\tilde{\mathbf{\Omega}}$ can be constructed when k, and m are known as shown in (18) and $\alpha_{j,\mu}^d$ is given by the right-hand side of (25). In this algorithm, the MF information is taken into account only through the prior and not through the observation term, whereas (26) also holds as far as the estimation of γ_j is concerned (for both the stationary and the nonstationary versions of the proposed prior). Moreover, in Algorithm 3 *simultaneous SR (and restoration) of all the HR frames is taking place*, which is not the case with Algorithms 1 and 2. More specifically, the main difference between Algorithms 2 and 3 is that in the former one only the part of the motion information which is relevant to the middle, kth, frame is incorporated in the fidelity term, whereas in the latter one all possible combinations of the motion field are used in the prior term. Consequently, in Algorithm 2, $(2m+1)$ frames are used in order to achieve SR (and restoration) of the middle frame only, whereas in Algorithm 3 all observed frames are simultaneously super-resolved (and restored).

As far as the stationary version of this algorithm is concerned, the minimization of the objective function results in

$$a_j = \frac{(LMLN-1)}{\|\mathbf{Q}\mathbf{f}_j\|^2},\ \beta_{ij} = \frac{LMLN}{\|\mathbf{f}_i - \mathbf{M}_{ij}\mathbf{f}_j\|^2} \tag{44}$$

$$(\tilde{\mathbf{G}} + \tilde{\mathbf{\Omega}}_{\mathrm{stat}})\hat{\tilde{\mathbf{f}}} = \tilde{\Lambda}\tilde{\mathbf{g}} \tag{45}$$

where $\tilde{\mathbf{\Omega}}_{\mathbf{stat}}$ is the stationary limiting case of $\tilde{\mathbf{\Omega}}$ which results from setting $l_i^d \to \infty$ and $\xi_{ij} \to \infty$ in (25) and (40). Based on the aforementioned analysis, in this case $\mathbf{A}_i^d = \alpha_i\mathbf{I}$, $\mathbf{B}_{ij} = \beta_{ij}\mathbf{I}$, and $\mathbf{Q}^d$ reduces to $\mathbf{Q}$ (discrete Laplacian).

The proposed algorithm can be illustrated step by step as follows.

Algorithm 3: Proposed/New SR method

Given an initial estimate for each HR image

1) Estimate all possible MFs
2) Estimate $\alpha_{j,\mu}^d$ using (25) -nonstationary prior- or α_j based on the left-hand side of (44) -stationary prior-
3) Estimate $\beta_{ij,\mu}$ using (40) -nonstationary prior- or β_{ij} based on the right-hand side of (44) -stationary prior-
4) Estimate γ_j using (26)
5) Based on steps 1), 2), 3) and 4) *simultaneously estimate all HR frames* using (41) -nonstationary prior- or (45) -stationary prior-

Since matrices $\mathbf{D}$, $\mathbf{D}^T$, $\mathbf{M}_{ij}$, $\mathbf{A}_j^d$, and $\mathbf{B}_{ij}$ are not block-circulant, and therefore they cannot be easily inverted due to their sizes, we resorted to numerical solutions of (27), (29), (34), (37), (41), and (45) using a *conjugate-gradient (CG) algorithm* [42].

IV. Experimental Results

In this section, we assess experimentally the performance of the proposed novel (state-of-the-art) MAP SR Algorithms 1, 2, and 3 in both their stationary and nonstationary forms and compare the proposed nonstationary Algorithm 3 with three other SR techniques in [10], [14], and [15]. Consecutive frames of the video sequences "Mobile" and "Bus" were used in experiments 1 and 2, similarly to [22] and [24]. More specifically, in the former case we use the central 316×316 region of each frame, whereas in the latter one we also utilize the central 256×256 region of each image. Moreover, all of the presented results were achieved by setting $m = 2$ for both sequences; frames "018"–"022" were used for the "Mobile" sequence and frames "111"–"115" for the "Bus" sequence.

For all sets of experiments 1 and 2, two cases were considered. In the first one, the selected frames of both sequences were degraded by uniform 9×9 blur, whereas in the second one no blur was used ($\mathbf{H} = \mathbf{I}$). For this latter case, we also compared the performance of the nonstationary Algorithm 3 to that of the SR algorithms proposed by [10], [14], and [15] (which is a representative IBP SR algorithm used in several frequently cited publications), which were implemented using the software provided by their authors. After blurring, subsampling by a factor of two $(L = 2)$ in both spatial dimensions took place and white Gaussian noise was added such that the blurred signal-to-noise ratio (BSNR) defined (in decibels) as

$$\mathrm{BSNR} = 10\log_{10}\left(\|\overline{\mathbf{DHf}}_i - \mathbf{DHf}_i\|^2 / \left(MN\gamma_i^{-1}\right)\right) \tag{46}$$

or, equivalently, the SNR when $\mathbf{H} = \mathbf{I}$, for each LR frame equals to 20, 30, and 40 dB ($\overline{\mathbf{DHf}}_i$ denotes the spatial mean of $\mathbf{DHf}_i$).

The objective metric used to quantify the quality of the results in the aforementioned experiments, is the improvement in signal-to-noise ratio (ISNR). This metric (in decibels) is defined as

$$\mathrm{ISNR} = 10\log_{10}\left(\|\mathbf{f}_i - \mathbf{g}_{i,I}\|^2 / \|\mathbf{f}_i - \hat{\mathbf{f}}_i\|^2\right) \tag{47}$$

where $\mathbf{g}_{i,I}$ denotes the bicubic interpolation of the i^{th} LR observation and $\hat{\mathbf{f}}_i$ is the respective estimated HR image.

Furthermore, we conducted experiment 3 in order to compare our proposed Algorithm 3 with respect to three existing SR techniques [10], [14], and [15] using two real datasets/sequences. The first one is the aforementioned "Bus" sequence, where frames "111"–"115" were also used (a central 128×128 region of each frame) and served directly as the LR observations of our algorithm (without being synthetically degraded) and also of the IBP SR algorithm which is proposed in [15]. The latter one is the "Disk" dataset taken from [18] where images "13"–"17" (whose central part with spatial dimension 49×49 was chosen) were used as the LR frames of both Algorithm 3 and the algorithm in [15]. We also note that based on [10] and [14], those SR methods utilize frames "113"–"116" from the "Bus" sequence (for the estimation of HR frame "113") and frames "15"–"18" from the "Disk" sequence (for the estimation of HR frame "15"). For both sequences, no blur [the unknown camera point spread function (PSF)] was used *for our proposed*

TABLE I
ISNR VALUES AND NUMBER OF CG ITERATIONS FOR MOBILE AND BUS FOR THE CASE OF 9×9 UNIFORM BLUR

		Mobile			Bus		
BSNR	Stationary Algorithm	ISNR (dB)	iterations	$\hat{\gamma}_k^{-1}$	ISNR (dB)	iterations	$\hat{\gamma}_k^{-1}$
$20dB$	1	1.55	415	13.46	1.96	506	16.90
$\gamma_{k,true-mob.}^{-1} = 11.98$	2	2.04	41	11.62	2.28	30	13.57
$\gamma_{k,true-bus}^{-1} = 13.77$	3	2.58	20	11.62	2.89	22	13.57
$30dB$	1	3.44	286	1.29	3.65	220	1.33
$\gamma_{k,true-mob.}^{-1} = 1.19$	2	3.55	21	0.83	3.75	22	0.94
$\gamma_{k,true-bus}^{-1} = 1.37$	3	4.17	19	0.83	4.07	20	0.94
$40dB$	1	4.76	165	0.14	4.37	180	0.10
$\gamma_{k,true-mob.}^{-1} = 0.12$	2	4.82	21	0.14	4.42	20	0.08
$\gamma_{k,true-bus}^{-1} = 0.13$	3	5.46	18	0.14	4.72	19	0.08

TABLE II
ISNR VALUES AND NUMBER OF CG ITERATIONS FOR MOBILE AND BUS FOR THE CASE OF NO BLUR/$\mathbf{H} = \mathbf{I}$

		Mobile			Bus		
SNR	Stationary Algorithm	ISNR (dB)	iterations	$\hat{\gamma}_k^{-1}$	ISNR (dB)	iterations	$\hat{\gamma}_k^{-1}$
$20dB$	1	1.93	245	17.93	2.05	267	20.04
$\gamma_{k,true-mob.}^{-1} = 14.19$	2	2.28	18	12.39	2.57	15	17.57
$\gamma_{k,true-bus}^{-1} = 19.55$	3	2.89	20	12.39	3.18	20	17.57
$30dB$	1	3.68	356	1.68	3.70	450	2.13
$\gamma_{k,true-mob.}^{-1} = 1.42$	2	3.80	16	1.12	3.80	10	1.54
$\gamma_{k,true-bus}^{-1} = 1.96$	3	4.31	20	1.12	4.33	19	1.54
$40dB$	1	4.13	650	0.50	3.84	650	0.35
$\gamma_{k,true-mob.}^{-1} = 0.14$	2	4.15	14	0.14	3.87	8	0.17
$\gamma_{k,true-bus}^{-1} = 0.20$	3	4.54	20	0.14	4.41	17	0.17

Algorithm 3 and for the IBP SR method in [15] (i.e., $\mathbf{H} = \mathbf{I}$), *whereas the formulation in* [10] and [14] *does not account for the possible presence of blur at all*. Moreover, in this experimental set, all reconstructed HR images have also a resolution enhancement factor of two $(L = 2)$. Clearly, in this set of experiments we cannot define objective metrics of performance such as the ISNR, given that the original frames are unknown. Therefore, the evaluation of the results provided by the SR methods is purely based on visual inspections.

In all experiments with Algorithms 2 and 3, the MF computation was performed using a three-level hierarchical block matching algorithm (HBMA) with integer pixel accuracy at each level [43]–[45], with *exhaustive* search for the motion vector computation at every pixel. The block dimensions were selected to be 5×5 at each resolution level, whereas an exhaustive search over an 11×11 area was used at each level, with matching metric the mean absolute difference (MAD). In all experiments, the convergence criterion used for the termination of the CG algorithm was $\|\mathbf{f}_k^{\text{new}} - \mathbf{f}_k^{\text{old}}\|^2 / \|\mathbf{f}_k^{\text{old}}\|^2 < 10^{-5}$, where $\mathbf{f}_k^{\text{new}} - \mathbf{f}_k^{\text{old}}$ represents the difference between two consecutive HR estimates. In the experiments that an iterative scheme was adopted, the entire process terminated when $\|\mathbf{f}_k^{\text{it}+1} - \mathbf{f}_k^{\text{it}}\|^2 / \|\mathbf{f}_k^{\text{it}}\|^2 < 10^{-7}$, where it denotes the iteration index. Moreover, for all algorithms, the results are presented with respect to the middle (kth) frame.

1) Experiment 1: In the first set of experiments, we tested the performance of the three algorithms in their *stationary* form. For Algorithm 1, the bicubically interpolated LR observations served as initial conditions. In all experiments with Algorithms 2 and 3 they (including the estimation of the parameters) are initialized by the results of Algorithm 1. Tables I and II report the ISNR values, the number of iterations and the values of the estimated noise variances for three different noise levels BSNR/SNR values, for the uniform blur and no blur cases, respectively. It has been experimentally demonstrated that when (28) is used for the estimation of the parameters a_i in Algorithms 1 and 2 for both cases of blur and also for both sequences, we obtain the best results in terms of ISNR when the aforementioned equation is scaled by a constant whose order of magnitude is 10^{-3}. Moreover, the same scaling is employed in Algorithm 3, where parameters α_j and β_{ij} are given by (44). The procedure of choosing the proper scaling constants has been also used in the past with success in video SR problems and also in image recovery problems [22], [46], [47].

Referring to Table I at low BSNR levels the improvement that Algorithm 3 provides over Algorithm 1, is much higher than the one at higher BSNR values. This can be attributed to the fact that the role of the prior becomes more important at low BSNRs [48]. Moreover, the lower the BSNR, the higher the margin of improvement which is achieved using Algorithms 2 and 3 with respect to Algorithm 1.

Finally, given Table II, all qualitative conclusions regarding the three algorithms also hold in the absence of blur as they have already been presented in the first set of experiments, proving that the use of the new multichannel prior is also efficient when addressing the SR problem by itself, i.e., there is no need for blur removal.

TABLE III
ISNR VALUES AND NUMBER OF CG ITERATIONS FOR MOBILE AND BUS FOR THE CASE OF 9 × 9 UNIFORM BLUR

		Mobile				Bus			
BSNR	Non-Stationary Algorithm	ISNR (dB)	iterations	l	ξ	ISNR (dB)	iterations	l	ξ
$20dB$	1	2.02	400	2.10	–	2.42	380	2.10	–
	2	2.33	40	2.10	–	2.63	42	2.10	–
	3	2.83	20	2.01	5	3.14	22	2.01	5
$30dB$	1	4.44	250	2.10	–	4.21	250	2.10	–
	2	4.45	28	2.10	–	4.25	26	2.10	–
	3	4.81	19	2.01	5	4.44	21	2.01	5
$40dB$	1	5.86	200	2.10	–	4.97	210	2.10	–
	2	5.93	19	2.10	–	5.07	10	2.10	–
	3	6.30	18	2.01	5	5.25	19	2.01	5

TABLE IV
ISNR VALUES AND NUMBER OF CG ITERATIONS FOR MOBILE AND BUS FOR THE CASE OF NO BLUR/$\mathbf{H} = \mathbf{I}$

		Mobile				Bus			
SNR	Non-Stationary Algorithm	ISNR (dB)	iterations	l	ξ	ISNR (dB)	iterations	l	ξ
$20dB$	1	2.97	300	2.10	–	2.95	380	2.10	–
	2	3.20	26	2.10	–	3.16	26	2.10	–
	3	3.71	19	2.01	5	3.86	21	2.01	5
	SR Algorithm in [14]	2.85	–	–	–	−0.35	–	–	–
	SR Algorithm in [10]	2.86	–	–	–	−0.12	–	–	–
	IBP SR Algorithm in [15]	1.51	30	–	–	−0.05	30	–	–
$30dB$	1	4.48	180	2.10	–	4.30	190	2.10	–
	2	4.58	24	2.10	–	4.40	20	2.10	–
	3	5.00	20	2.01	5	4.65	20	2.01	5
	SR Algorithm in [14]	3.22	–	–	–	−0.50	–	–	–
	SR Algorithm in [10]	3.19	–	–	–	−0.33	–	–	–
	IBP SR Algorithm in [15]	2.42	25	–	–	−0.10	26	–	–
$40dB$	1	4.94	150	2.10	–	4.45	155	2.10	–
	2	5.02	22	2.10	–	4.50	20	2.10	–
	3	5.31	20	2.01	5	4.70	20	2.01	5
	SR Algorithm in [14]	3.28	–	–	–	−0.55	–	–	–
	SR Algorithm in [10]	3.32	–	–	–	−0.37	–	–	–
	IBP SR Algorithm in [15]	2.55	25	–	–	−0.15	24	–	–

TABLE V
PERFORMANCE LIMITS IN TERMS OF ISNR VALUES FOR MOBILE FOR THE CASE OF 9 × 9 UNIFORM BLUR

		Mobile		Mobile
BSNR	Stationary Algorithm	ISNR (dB)	Non-Stationary Algorithm	ISNR (dB)
$20dB$	3	3.42	3	4.63
$30dB$	3	5.76	3	7.36
$40dB$	3	6.85	3	9.71

2) Experiment 2: In the second set of experiments, we evaluated the performance of the *nonstationary* versions of the three proposed algorithms. More specifically, the CG algorithm for each nonstationary algorithm was initialized by its respective stationary results based on which the MFs were also computed. As far as the hyperparameters are concerned, parameters ν_j^d were obtained as $\nu_j^d = 1/(2\alpha_{j\text{stat}})$, where $\alpha_{j\text{stat}}$ are the within channel parameters obtained by the respective stationary algorithms. These parameters were assumed to be equal for the two selected directions. As far as the τ_{ij}s in Algorithm 3 are concerned, they are expressed as $\tau_{ij} = 1/(2\beta_{ij\text{stat}})$, where $\beta_{ij\text{stat}}$ are the cross-channel precisions given by the respective stationary algorithms. The parameters l_j^d were selected to be all equal to a value denoted by l and within the same context parameters ξ_{ij} were equal to the value ξ. Using trial and error, values in the interval $l = [2.01 - 2.5]$ and $\xi = [2.01 - 5]$ were found to provide the best SR (and restoration) results based on both visual criteria and the adopted ISNR metric.

The results of this set of experiments (with respect to the kth frame) are summarized in Tables III and IV. Commenting on these tables in more detail, we come up with the same qualitative conclusions that we have already mentioned for Tables I and II. Overall, the experimental results demonstrate that Algorithm 3 in its nonstationary version clearly outperforms all

other algorithms for both cases of severe blur and no blur, for both sequences. Moreover, it is clear that the proposed multichannel prior yields high performance, proving that incorporating the MF information in the prior knowledge is much more helpful than using it in the observation term. Furthermore, the experiments proved that even when comparing the stationary algorithms among themselves, Algorithm 3 is clearly better and serves as a framework of initial conditions for the respective nonstationary algorithm. Finally, referring to Table IV, our proposed nonstationary Algorithm 3 clearly provides a superior performance as compared to the SR algorithms in [10], [14], and [15]. This is established quantitatively by the negative ISNR values that both algorithms exhibit in the case of "Bus" sequence, while in the case of "Mobile" sequence these values are lower even when compared to the respective values of stationary Algorithm 3. Moreover, based on the aforementioned table, the IBP SR method in [15] converges slower than the proposed Algorithm 3.

In order to test the performance limits of the proposed prior in both its stationary and nonstationary versions, we indicatively implemented the two versions of Algorithm 3 estimating the MFs and the precision parameters from the original images, whereas the CG algorithm was initialized by the restored frames exactly as it was done previously. For these experiments, we utilized the "Mobile" sequence in the 9×9 uniform blur case. From the SR frames shown in Figs. 1 and 2 along with the results shown in Table V, it is clear that the proposed *nonstationary* algorithms provide *both* higher ISNR values (by up to almost 3 dB for the case of 40 dB BSNR) and visually much more accurate and pleasing results than the corresponding stationary algorithms.

Some indicative visual proof of the aforementioned conclusions are presented in the figures of this paper. As far as the efficacy of the stationary Algorithm 3 is concerned, as can be seen in Figs. 1(e), 2(d), and 4(c), several areas of the middle frame of the "Mobile" sequence benefit from the recovery i.e., the numbers in the calendar are sharper and all other image areas are also improved. Based also on the visual results, of Figs. 1(f), 2(e), 3(e), and 4(d), the nonstationary version of Algorithm 3 further improves the image in the sense that ringing artifacts are removed at all noise levels and the edges become sharper. Furthermore, resolution enhancement is increased (especially for high (B)SNR values) due to the better utilization of the MF information. Moreover, comparison among Fig. 4(c)–(g) further establishes the efficacy of our proposed algorithm with respect to the SR techniques in [10], [14], and [15]. Finally, the superiority of nonstationary Algorithm 3 becomes more clear by the comparison of Fig. 3(e)–(h) where the aforementioned algorithms obviously fail to accurately estimate the motion, especially in the iron fence region. In all cases, the results obtained by the IBP method have more noise and artifacts, compared to all the other methods. Based on [49], the same conclusions are drawn for the POCS SR algorithms described in [17] and [50].

3) Experiment 3: In this experimental set, we compare the results of our proposed method (nonstationary Algorithm 3) with three other SR techniques [10], [14], and [15], using two real sequences, the "Bus" and the "Disk" sequences. As far as our algorithm is concerned it was implemented as it has already been explained (it is noted that parameters l and ξ were chosen to be equal to 2.01 and 5, respectively). Moreover, in the implementation of the techniques proposed in [10], [14], and [15], upsampling was performed using bicubic interpolation. As men-

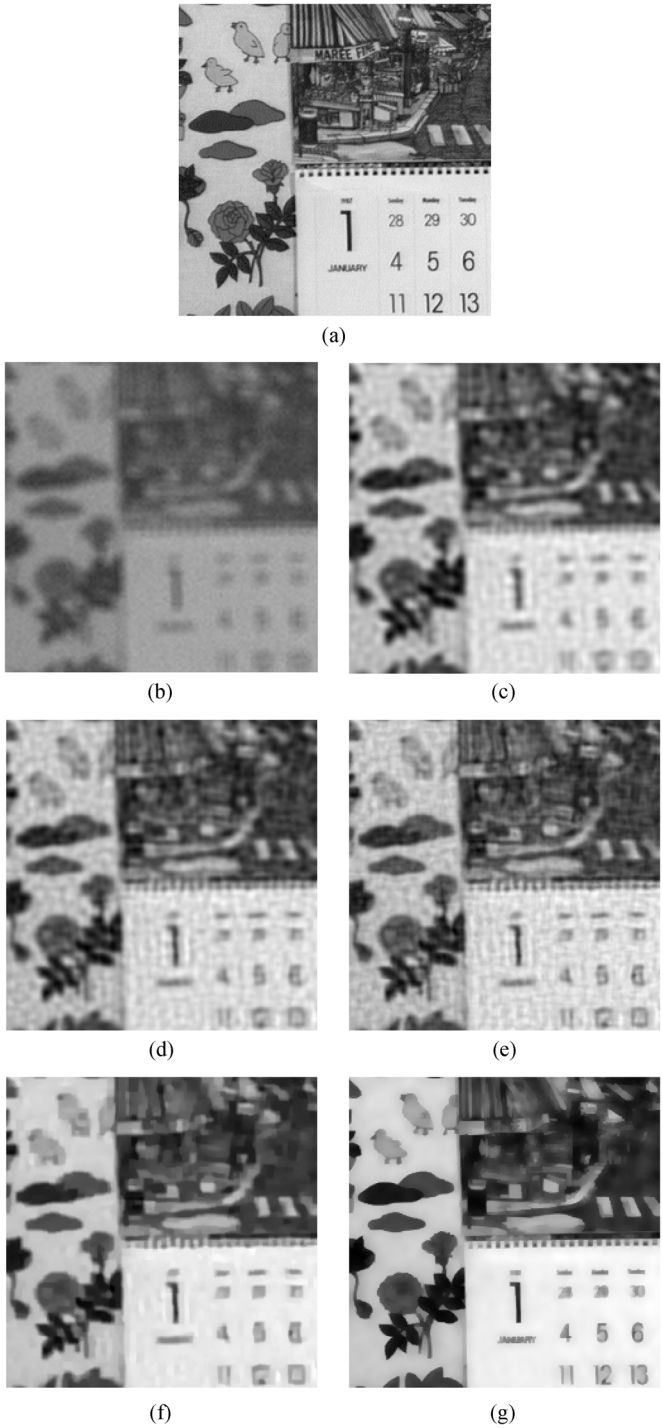

Fig. 1. (a) Original middle frame (central segment) of the "Mobile" sequence. SR estimates of the respective frame with a 9×9 uniform PSF (Case of BSNR = 20 dB). Result after (b) bicubic interpolation of the LR observation, (c) stationary Algorithm 1 method (ISNR = 1.55 dB), (d) stationary Algorithm 2 method (ISNR = 2.04 dB), (e) stationary Algorithm 3 method (ISNR = 2.58 dB), (f) nonstationary Algorithm 3 method (ISNR = 2.83 dB), and (g) testing the performance limits of the nonstationary Algorithm 3 (ISNR = 4.63 dB/Table V).

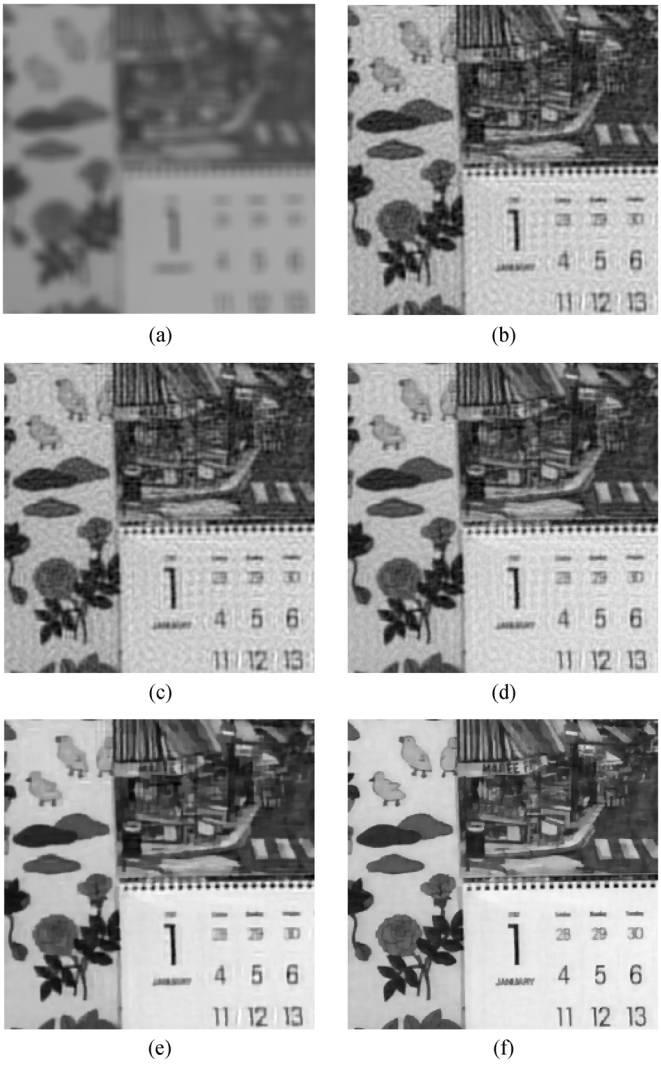

Fig. 2. Middle frame (central segment) SR estimates of the "Mobile" sequence with a 9×9 uniform PSF (Case of BSNR = 40 dB). Result after (a) bicubic interpolation of the LR observation, (b) stationary Algorithm 1 method (ISNR = 4.76 dB), (c) stationary Algorithm 2 method (ISNR = 4.82 dB), (d) stationary Algorithm 3 method (ISNR = 5.46 dB), (e) nonstationary Algorithm 3 method (ISNR = 6.30 dB), and (f) testing the performance limits of the nonstationary Algorithm 3 (ISNR = 9.71 dB/Table V).

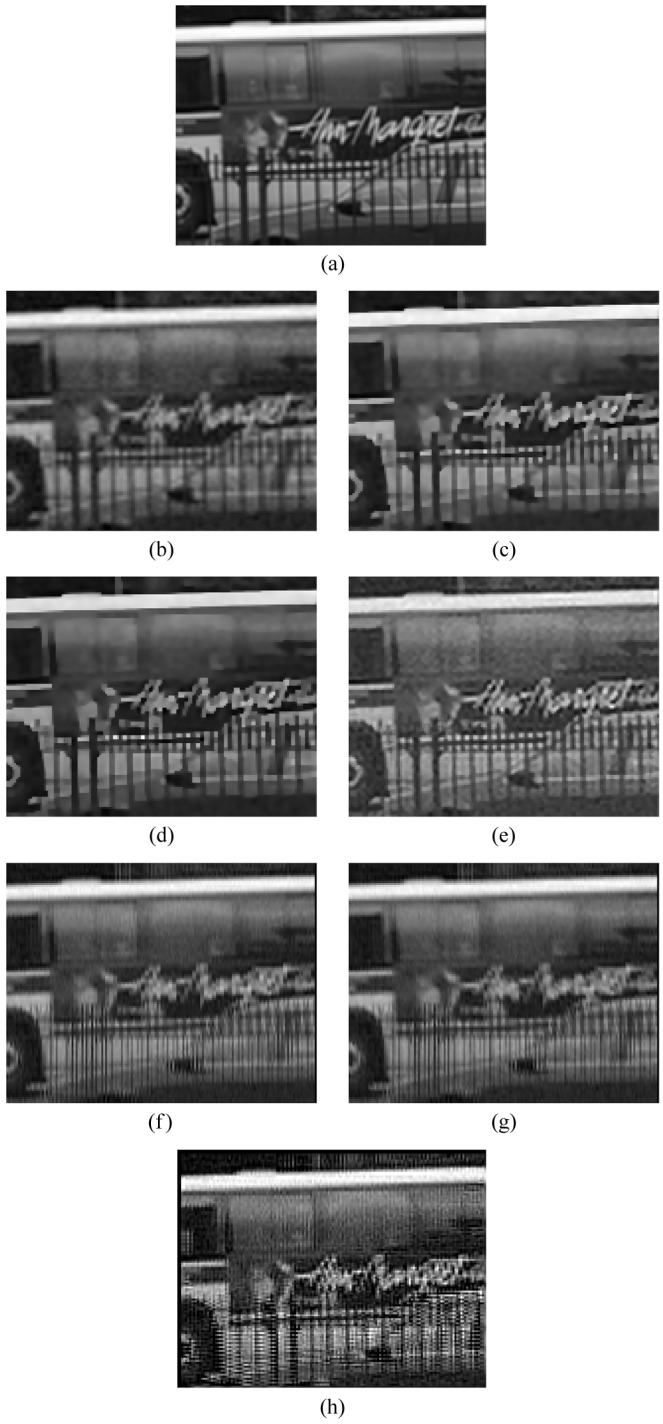

Fig. 3. (a) Original middle frame (central segment) of the "Bus" sequence. SR estimates of the respective frame with no blur/$\mathbf{H} = \mathbf{I}$ (Case of SNR = 20 dB). Result after (b) bicubic interpolation of the LR observation, (c) nonstationary Algorithm 1 method (ISNR = 2.05 dB), (d) nonstationary Algorithm 2 method (ISNR = 2.57 dB), (e) nonstationary Algorithm 3 method (ISNR = 3.18 dB), (f) SR algorithm proposed in [14] (ISNR = -0.35 dB), (g) SR algorithm proposed in [10] (ISNR = -0.12 dB), and (h) IBP SR algorithm proposed in [15] (ISNR = -0.05 dB).

tioned previously our algorithm can estimate nonuniform motion, whereas the algorithms in [10], [14], and [15] assume uniform motion and rotation (the method in [15] tracks multiple independent motions assuming an affine motion model). The motion in the "Bus" sequence is not uniform, while the motion in the "Disk" is. As a result the motion model of our algorithm fits well to the "Bus" sequence, while the motion model of [10], [14], and [15] fits well the "Disk" sequence.

The results of this experiment are shown in Figs. 5 and 6. From these results, we observe that the proposed method clearly outperforms the methods in [10], [14], and [15] for the "Bus" sequence. As far as the "Disk" sequence is concerned whose motion clearly favors the SR algorithms in [10], [14], and [15], our method provided comparable performance with them. In all cases, our algorithm outperforms bicubic interpolation.

In terms of computational cost, all proposed algorithms were quite fast. Typically, the CG algorithm required about 20–40 iterations to converge. In the experiments that an iterative scheme was adopted, the entire process terminated after about 10–15 iterations. All experiments were performed using MATLAB on a 2.33 GHz personal computer. All calculations for the implementation of the CG method for all algorithms required 1–1.5 min, whereas the total time required for the computation of the MFs

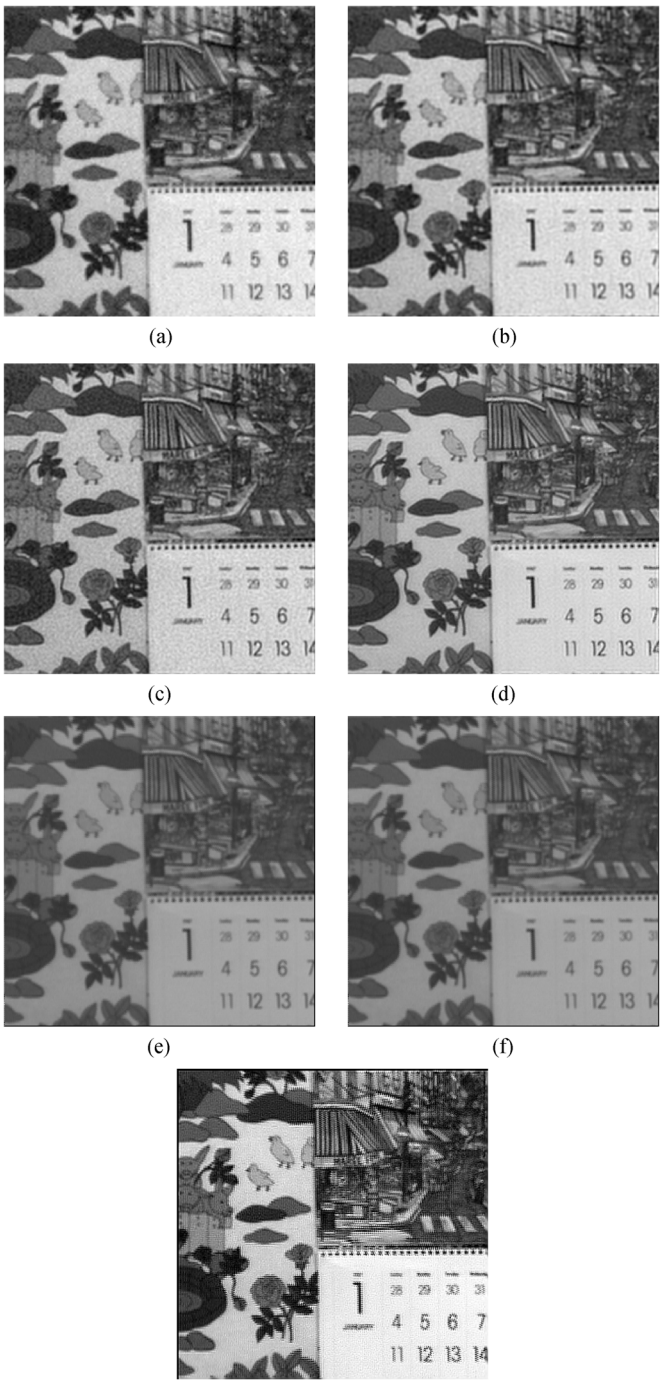

Fig. 4. Middle frame SR estimates of the "Mobile" sequence with no blur/$\mathbf{H} = \mathbf{I}$ (Case of SNR = 30 dB). Result after (a) bicubic interpolation of the LR observation, (b) stationary Algorithm 1 method (ISNR = 3.68 dB), (c) stationary Algorithm 3 method (ISNR = 4.31 dB), (d) nonstationary Algorithm 3 method (ISNR = 5.00 dB), (e) SR algorithm proposed in [14] (ISNR = 3.22 dB), (f) SR algorithm proposed in [10] (ISNR = 3.19 dB), and (g) IBP SR algorithm proposed in [15] (ISNR = 2.42 dB).

Fig. 5. (a) LR middle frame (central segment) of the "Bus" sequence. Corresponding frame SR estimates. Result after (b) bicubic interpolation of the LR observation, (c) SR algorithm proposed in [14], (d) SR algorithm proposed in [10], (e) our proposed SR algorithm (nonstationary Algorithm 3), and (f) IBP SR algorithm proposed in [15].

(20 of them for the five-channel window used in Algorithm 3) is almost 20 min. This time depends on the frame size. The estimation of the inverse variance parameters took less than 1 min. Finally, we also tested both sequences ("Mobile" and "Bus") by implementing the experiments not only for a five-frame sequence, but also using 3, 7, and 9 frames. The best results in terms of ISNR and visually were obtained for the five-channel case when using all possible combinations ($|i-j| \leqq 4$), for the seven-channel case when $|i-j| \leqq 3$ and for the nine-channel case when $|i-j| \leqq 2$. These results were similar among themselves and clearly better than the three-channel case. These experiments demonstrated that the larger the frame window size, the smaller the maximum neighborhood size of the pairs of frames which are used in the proposed prior should be.

V. Conclusion and Future Research

In this paper, we presented a MAP approach that utilizes a *new multichannel image prior*, and both its nonstationary and stationary forms were applied to the digital video SR problem. We also compared the novel proposed algorithm with two other

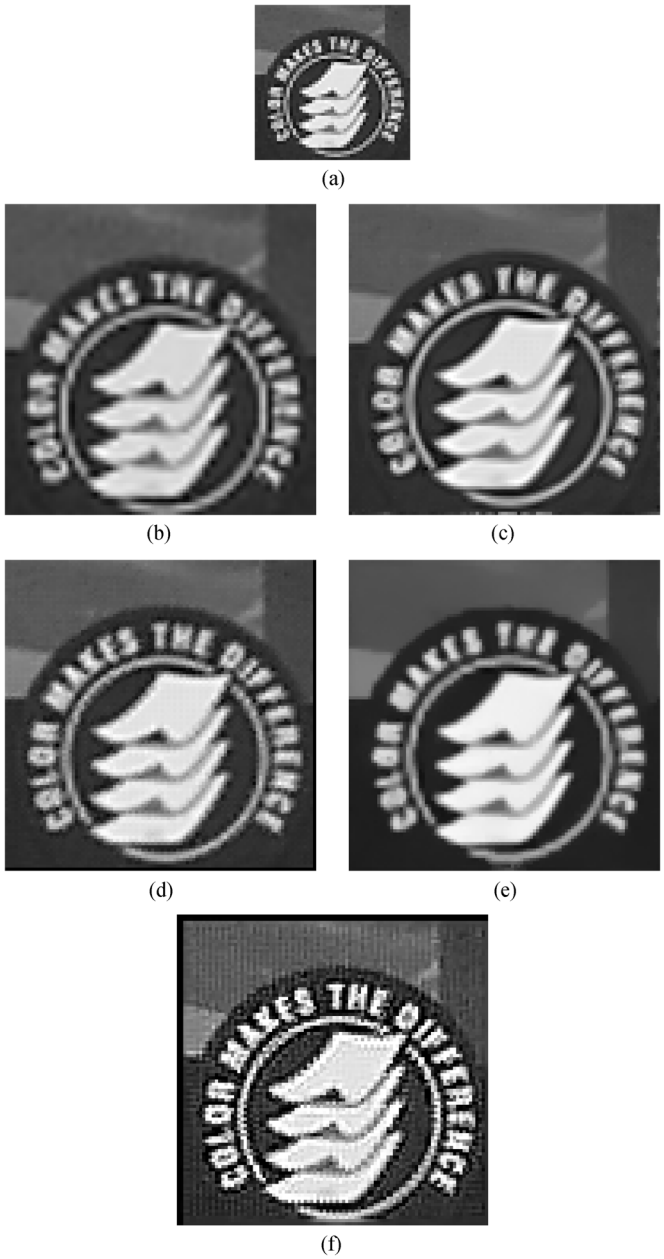

Fig. 6. (a) LR middle frame (central segment) of the "Disk" sequence. Corresponding frame SR estimates. Result after (b) bicubic interpolation of the LR observation, (c) SR algorithm proposed in [14], (d) SR algorithm proposed in [10], (e) our proposed SR algorithm (nonstationary Algorithm 3), and (f) IBP SR algorithm proposed in [15].

algorithms we propose. Moreover, we tested our new algorithm with the three SR techniques in [10], [14], and [15], for certain experimental cases, using also real video data. The proposed algorithms were tested for different cases (presence and absence of blur for different BSNR and SNR values). The experimental results showed that in all cases the algorithm which utilizes the *nonstationary* version of the new proposed prior (Algorithm 3) *performs better* than nonstationary Algorithms 1 and 2 in terms of both *visual quality and improvement in* SNR/ISNR. Furthermore, the comparison between Algorithms 2 and 3 provides a strong indication that the use of MF in the prior term is much more effective in terms of both restoration and resolution enhancement capability than its use in the observation term. Moreover, our method provided in most cases a superior, and in one only case at least as good, of a performance as the SR techniques in [10], [14], and [15].

Nevertheless, we plan to investigate whether we can further improve the proposed algorithms by introducing a new model, that uses a TV based prior [25].

REFERENCES

[1] A. K. Katsaggelos, Ed., *Digital Image Restoration*. New York: Springer-Verlag, 1991, vol. 23.
[2] M. R. Banham and A. K. Katsaggelos, "Digital image restoration," *IEEE Signal Process. Mag.*, vol. 14, no. 2, pp. 24–41, Mar. 1997.
[3] P. Sarder and A. Nehorai, "Deconvolution methods for 3-D fluorescence microscopy images: An overview," *IEEE Signal Process. Mag.*, vol. 23, no. 3, pp. 32–45, May 2006.
[4] A. K. Katsaggelos, R. Molina, and J. Mateos, *Super Resolution of Images and Video*. San Rafael, CA: Morgan & Claypool, 2007.
[5] S. Borman and R. L. Stevenson, "Super-resolution from image sequences—A review," in *Proc. Midwest Symp. Circuits Systems*, Notre Dame, IN, Apr. 1998, vol. 5, pp. 374–378.
[6] C. Kim, M. Kang, S. Cho, S. Oh, H. Park, and M. Park, "Noise insensitive demosaicing algorithm," in *Proc. IASTED Int. Conf. Signal Image Processing (SIP 2007)*, Honolulu, HI, Aug. 20–22, 2007, pp. 422–427.
[7] R. Y. Tsai and T. S. Huang, "Multi-frame image restoration and registration," *Adv. Comput. Vis. Image Process.*, vol. 1, no. 1, pp. 317–339, 1984.
[8] S. P. Kim, N. K. Bose, and H. M. Valenzuela, "Recursive reconstruction of high resolution image from noisy undersampled multiframes," *IEEE Trans. Acoust., Speech, Signal Process.*, vol. 38, no. 2, pp. 1013–1027, Jun. 1990.
[9] N. K. Bose, H. C. Kim, and H. M. Valenzuela, "Recursive total least squares algorithm for image reconstruction from noisy, undersampled frames," *Multidimension. Syst. Signal Process.*, vol. 4, no. 3, pp. 253–268, 1993.
[10] P. Vandewalle, S. E. Süsstrunk, and M. Vetterli, "A frequency domain approach to registration of aliased images with application to super-resolution," *EURASIP J. Appl. Signal Process.*, vol. 2006, pp. 1–14, 2006.
[11] B. S. Reddy and B. N. Chatterji, "An FFT-based technique for translation, rotation, and scale-invariant image registration," *IEEE Trans. Image Process.*, vol. 5, no. 8, pp. 1266–1271, Aug. 1996.
[12] L. Lucchese and G. M. Cortelazzo, "A noise-robust frequency domain technique for estimating planar roto-translations," *IEEE Trans. Signal Process.*, vol. 48, no. 6, pp. 1769–1786, Jun. 2000.
[13] S. C. Park, M. K. Park, and M. G. Kang, "Super-resolution image reconstruction: A technical overview," *IEEE Signal Process. Mag.*, vol. 20, no. 3, pp. 21–36, May 2003.
[14] D. Keren, S. Peleg, and R. Brada, "Image sequence enhancement using sub-pixel displacements," presented at the IEEE Int. Conf. Computer Vision Pattern Recognition (CVPR), Ann Arbor, MI, Jun. 1988.
[15] M. Irani and S. Peleg, "Motion analysis for image enhancement: Resolution, occlusion, and transparency," *J. Vis. Commun. Image Represent.*, vol. 4, no. 4, p. 1993-12, 1993.
[16] H. Stark and P. Oskoui, "High-resolution image recovery from image-plane arrays, using convex projections," *J. Opt. Soc. Amer. A, Opt. Image Sci., Vis.*, vol. 6, no. 11, pp. 1715–1726, 1989.
[17] A. M. Tekalp, M. K. Ozkan, and M. I. Sezan, "High-resolution image reconstruction from lower-resolution image sequences and space-varying image restoration," presented at the IEEE Int. Conf. Acoustics, Speech, Signal Processing (ICASSP), San Francisco, CA, 1992.
[18] S. Farsiu, M. D. Robinson, M. Elad, and P. Milanfar, "Fast and robust multiframe super resolution," *IEEE Trans. Image Process.*, vol. 13, no. 10, pp. 1327–1344, Oct. 2004.
[19] H. Shen, L. Zhang, B. Huang, and P. Li, "A MAP approach for joint motion estimation, segmentation, and super resolution," *IEEE Trans. Image Process.*, vol. 16, no. 2, pp. 479–490, Feb. 2007.
[20] R. R. Schultz and R. L. Stevenson, "Extraction of high-resolution frames from video sequences," *IEEE Trans. Image Process.*, vol. 5, no. 6, pp. 996–1011, Jun. 1996.
[21] H. Ji and C. Fermüller, "Wavelet-based super-resolution reconstruction: Theory and algorithm," in *Proc. Eur. Conf. Computer Vision (ECCV)*, vol. 3954, Lecture Notes in Computer Science, pp. 295–307.
[22] C. A. Segall, A. K. Katsaggelos, R. Molina, and J. Mateos, "Bayesian resolution enhancement of compressed video," *IEEE Trans. Image Process.*, vol. 13, no. 7, pp. 898–911, Jul. 2004.
[23] C. A. Segall, R. Molina, and A. K. Katsaggelos, "High-resolution images from low-resolution compressed video," *IEEE Signal Process. Mag.*, vol. 20, no. 3, pp. 37–48, May 2003.

[24] C. Wang, P. Xue, and W. Lin, "Improved super-resolution reconstruction from video," *IEEE Trans. Circuits Syst. Video Technol.*, vol. 16, no. 11, pp. 1411–1422, Nov. 2006.
[25] M. K. Ng, H. Shen, E. Y. Lam, and L. Zhang, "A total variation regularization based super-resolution reconstruction algorithm for digital video," *EURASIP J. Adv. Signal Process.*, vol. 2007, pp. 1–16, 2007.
[26] J. Bioucas-Dias, M. Figueiredo, and J. Oliveira, "Adaptive total-variation image deconvolution: A majorization-minimization approach," presented at the EUSIPCO 2006, Florence, Italy, Sep. 2006.
[27] S. D. Babacan, R. Molina, and A. K. Katsaggelos, "Parameter estimation in TV image restoration using variational distribution approximation," *IEEE Trans. Image Process.*, vol. 17, no. 3, pp. 326–339, Mar. 2008.
[28] M. C. Hong, T. Stathaki, and A. K. Katsaggelos, "Iterative regularized least-mean mixed-norm multichannel image restoration," *Opt. Eng.*, vol. 41, no. 10, pp. 2515–2524, Oct. 2002.
[29] N. P. Galatsanos and R. T. Chin, "Digital restoration of multichannel images," *IEEE Trans. Acoust., Speech, Signal Process.*, vol. 37, no. 3, pp. 415–421, Mar. 1989.
[30] M. G. Choi, N. P. Galatsanos, and A. K. Katsaggelos, "Multichannel regularized iterative restoration of motion compensated image sequences," *J. Vis. Commun. Image Represent.*, vol. 7, no. 3, pp. 244–258, Mar. 1996.
[31] M. G. Choi, Y. Yang, and N. P. Galatsanos, "Multichannel regularized recovery of compressed video sequences," *IEEE Trans. Circuits Syst. II, Analog Digit. Signal Process.*, vol. 48, no. 4, pp. 376–387, Apr. 2001.
[32] G. K. Chantas, N. P. Galatsanos, and A. C. Likas, "Bayesian restoration using a new nonstationary edge-preserving image prior," *IEEE Trans. Image Process.*, vol. 15, no. 10, pp. 2987–2997, Oct. 2006.
[33] M. Elad and Y. Hel-Or, "A fast super-resolution reconstruction algorithm for pure translational motion and common space-invariant blur," *IEEE Trans. Image Process.*, vol. 10, no. 8, pp. 1187–1193, Aug. 2001.
[34] N. Nguyen, P. Milanfar, and G. Golub, "A computationally efficient superresolution image reconstruction algorithm," *IEEE Trans. Image Process.*, vol. 10, no. 4, pp. 573–583, Apr. 2001.
[35] J. P. Noonan and P. Natarajan, "A general formulation for iterative restoration methods," *IEEE Trans. Acoust., Speech, Signal Process.*, vol. 45, no. 10, pp. 2590–2593, Oct. 1997.
[36] G. K. Chantas, N. P. Galatsanos, A. C. Likas, and M. Saunders, "Variational Bayesian image restoration based on a product of t-distributions image prior," *IEEE Trans. Image Process.*, vol. 17, no. 10, pp. 1795–1805, Oct. 2008.
[37] R. Molina, "On the hierarchical Bayesian approach to image restoration: Applications to astronomical images," *IEEE Trans. Pattern Anal. Mach. Intell.*, vol. 16, no. 11, pp. 1122–1128, Nov. 1994.
[38] J. M. Bernardo and A. F. M. Smith, *Bayesian Theory*. New York: Wiley, 2000.
[39] N. P. Galatsanos, V. Z. Mesarovic, R. Molina, J. Mateos, and A. K. Katsaggelos, "Hyper-parameter estimation using gamma hyper-priors in image restoration from partially-known blurs," *Opt. Eng.*, vol. 41, no. 8, pp. 1845–1854, Aug. 2002.
[40] J. Berger, *Statistical Decision Theory and Bayesian Analysis*. New York: Springer, 1993.
[41] M. E. Tipping, "Sparse Bayesian learning and the relevance vector machine," *J. Mach. Learn. Res.*, vol. 1, pp. 211–244, 2001.
[42] J. Nocedal and S. J. Wright, *Numerical Optimization*. New York: Springer-Verlag, 1999.
[43] Y. Wang, Y. Q. Zhang, and J. Ostermann, *Video Processing and Communications*. Englewood Cliffs, NJ: Prentice-Hall, 2001.
[44] B. Liu and A. Zaccarin, "New fast algorithms for the estimation of block motion vectors," *IEEE Trans. Circuits Syst. Video Technol.*, vol. 3, no. 2, pp. 148–157, Feb. 1993.
[45] A. M. Tekalp, *Digital Video Processing*. Englewood Cliffs, NJ: Prentice-Hall, 1995.
[46] M. G. Kang and A. K. Katsaggelos, "General choice of the regularization functional in regularized image restoration," *IEEE Trans. Image Process.*, vol. 4, no. 5, pp. 594–602, May 1995.
[47] R. L. Lagendijk, J. Biemond, and D. E. Boekee, "Regularized iterative image restoration with ringing reduction," *IEEE Trans. Acoust., Speech, Signal Process.*, vol. 36, no. 12, pp. 1874–1888, Dec. 1988.
[48] S. M. Kay, *Fundamentals of Statistical Signal Processing: Estimation Theory*. Englewood Cliffs, NJ: Prentice-Hall, 1993, vol. I.
[49] B. K. Gunturk, Y. Altunbasak, and R. M. Mersereau, "Multiframe resolution-enhancement methods for compressed video," *IEEE Signal Process. Lett.*, vol. 9, no. 6, pp. 170–174, Jun. 2002.
[50] M. Elad and A. Feuer, "Restoration of a single superresolution image from several blurred, noisy, and undersampled measured images," *IEEE Trans. Image Process*, vol. 6, no. 12, pp. 1646–1658, Dec. 1997.

Stefanos P. Belekos (S'08–M'10) was born in Athens, Greece, in 1979. He received the B.Sc. degree in physics, and the M.Sc. degree (with Distinction) in telecommunications and electronics from the National and Kapodistrian University of Athens, Athens, Greece, in 2001 and 2003, respectively, the M.Sc. degree (with Distinction) in satellite communication engineering from the Electronic Engineering Department, University of Surrey, Guildford, U.K., in 2004, and the Ph.D. degree in Bayesian algorithms for video (compressed and noncompressed) super-resolution and restoration, from the Faculty of Physics, Department of Electronics, Computers, Telecommunications and Control at the National and Kapodistrian University of Athens in 2009.

In 2008 and 2009, he was a Research Assistant (Predoctoral Fellow) in the Image and Video Processing Laboratory, Department of Electrical Engineering and Computer Science, at Northwestern University, Evanston, IL. He has been a Research Assistant with the Electronics and Telecommunications Laboratory and a Teaching Assistant for a course in digital signal processing, at the National and Kapodistrian University of Athens from 2005 to 2009. He is currently a Core Network Engineer at Vodafone, Athens, Greece. His primary research interests are in the areas of statistical video processing and include video restoration and resolution enhancement, video compression, and super-resolution.

Nikolaos P. Galatsanos (SM'95) received the Diploma degree in electrical engineering from the National Technical University of Athens, Greece, in 1982 and the M.S.E.E. and Ph.D. degrees from the Electrical and Computer Engineering Department of the University of Wisconsin—Madison in 1984 and 1989, respectively.

From 1989 to 2002, he was on the faculty of the Electrical and Computer Engineering Department at the Illinois Institute of Technology, Chicago. From 2002 to 2007, he was with the Department of Computer Science, University of Ioannina, Ioannina, Greece. Since 2007, he has been with the Department of Electrical and Computer Engineering of the University of Patras, Patras, Greece. He co-edited a book titled *Image Recovery Techniques for Image and Video Compression and Transmission* (Kluwer Academic, 1998). His research interests center around Bayesian methods for image processing, medical imaging, bioinformatics, and visual communications applications.

Dr. Galatsanos has served as an Associate Editor for the IEEE TRANSACTIONS ON IMAGE PROCESSING, the *IEEE Signal Processing Magazine*, the *Journal of Electronic Imaging*, and the IEEE SIGNAL PROCESSING LETTERS.

Aggelos K. Katsaggelos (S'80–M'85–SM'92–F'98) received the Diploma degree in electrical and mechanical engineering from the Aristotelian University of Thessaloniki, Greece, in 1979 and the M.S. and Ph.D. degrees in electrical engineering from Georgia Institute of Technology, Atlanta, in 1981 and 1985, respectively.

In 1985, he joined the Electrical Engineering and Computer Science Department at Northwestern University, Evanston, IL, where he is currently a Professor. He was the holder of the Ameritech Chair of Information Technology from 1997 to 2003. He is also the Director of the Motorola Center for Seamless Communications, a member of the Academic Staff, the NorthShore University Health System, and an affiliated faculty member at the Department of Linguistics and the Argonne National Laboratory. He has published extensively, and he is the holder of 16 international patents. He is the coauthor of *Rate-Distortion Based Video Compression* (Kluwer, 1997), *Super-Resolution for Images and Video* (Claypool, 2007), and *Joint Source-Channel Video Transmission* (Claypool, 2007).

Dr. Katsaggelos was Editor-in-Chief of the *IEEE Signal Processing Magazine* from 1997 to 2002, a BOG Member of the IEEE Signal Processing Society from 1999 to 2001, and a member of the Publication Board of the *IEEE Proceedings* from 2003 to 2007, among his many professional activities. He is a Fellow of the SPIE (2009) and the recipient of the IEEE Third Millennium Medal (2000), the IEEE Signal Processing Society Meritorious Service Award (2001), an IEEE Signal Processing Society Best Paper Award (2001), an IEEE ICME Paper Award (2006), an IEEE ICIP Paper Award (2007), and an ISPA Paper Award (2009). He was a Distinguished Lecturer of the IEEE Signal Processing Society from 2007 to 2008.